III European Conference on Computational Mechanics
Solids, Structures and Coupled Problems in Engineering
C.A. Mota Soares et.al. (eds.)
Lisbon, Portugal, 5–8 June 2006

SENSITIVITY OF BLOOD FLOW PATTERNS TO THE CONSTITUTIVE LAW OF THE FLUID

Pablo J. Blanco[1], **Ignacio Larrabide**[1], **Santiago A. Urquiza**[2], **Raúl A. Feijóo**[1]

[1]Laboratório Nacional de Computação Científica - LNCC
Rua Getulio Vargas 333, 25651-057, Petropolis, RJ, Brazil
address
pjblanco, nacho, feij@lncc.br

[2] Laboratorio de Bioingeniería, Universidad Nacional de Mar del Plata
Av. J.B. Justo 4302, 7600, Mar del Plata, Argentina
address
santiagourquiza@fi.mdp.edu.ar

Keywords: Hemodynamics, Blood flow, Constitutive law, Sensitivity, Coupling 3D-1D.

Abstract. *It is well known that hemodynamic factors are strongly influenced by the arterial geometry. Combining computational fluid dynamics with three-dimensional medical data makes possible the study of blood flow in real geometries. By this means we are able to analyze the sensitivity of hemodynamic factors due to shape changes in vascular districts. It is also well known that the fluid's constitutive law very much influences the flow structure in singularities, such as the carotid sinus. In this work we quantify the sensitivity of blood flow for a model of a carotid bifurcation due to different constitutive behavior. In this case, the flow pattern for the Casson constitutive equation for the fluid is compared with its Newtonian counterpart. To this end a multidimensional 3D-1D FEM model of the whole arterial tree is implemented. It comprises a 3D compliant model of the carotid bifurcation coupled with a 1D model for the remaining part of the arterial tree. With this approach, difficulties arising from the treatment of boundary conditions for the 3D model are naturally handled. In particular, two carotid bifurcation geometries were analyzed. One of them corresponds to a standard model taken from literature. The second geometry was acquired from a patient-specific angiography using image segmentation and reconstruction techniques. Detailed hemodynamic factors and flow patterns in the carotid bifurcation are provided. Finally, this data is analyzed in order to determine how these results are affected in the different cases under study.*

1 INTRODUCTION

Several efforts have been made so as to prevent and diagnose vascular diseases through using computational tools in the past few years. In this regard, atheroma plaques deposition is one of the prevalent pathologies, and recent studies reveal that atherosclerosis tend to be placed where irregular hemodynamic conditions are present. Such irregular conditions refer to complex blood flow patterns as those observed at singularities such as bifurcations or highly-curved districts. These regions have a tendency to be characterized by the presence of high flow reversal zones and low oscillating stresses as well [14, 15, 16]. Since most of the times it is not convenient to perform *in vivo* experiments, computational modelling have played an important role in giving support to this field of research.

In this way, with the help of computational advances, it is possible to develop computational models that account for the different phenomena present in the human arterial tree without inconveniencing people. Thus, when tackling such kind of problems we face a multi-physics problem for which the level of detail may go from celular physics to fluid mechanics. Hence, we are interested in a macro-modelling point of view, that is, a model that accounts for the blood behavior will be adopted, and therefore we will use the fluid mechanics equations as our physic model. In this context, we have to deal with the reconstruction of geometries from medical images (or standard geometries), as well as with the numerical solution of highly non-linear problems comprising fluid-structure interaction and the coupling between models of different dimensionality [4, 12, 13]. Particularly, in this last approach a detailed model interacts with lumped models expressing the systemic interaction between the whole arterial tree and the district where more detail of the flow characteristics is desired. By detailed model we mean multidimensional 2D or 3D models. Hence, different situations of interest can be tested without knowing *a priori* modified boundary data for the multidimensional districts. This simplifies the implementation and analysis, for example, of different degrees of stenosis at a particular point within the arterial tree [19, 21].

Another source of research is the blood behavior, and how it affects hemodynamics. Different constitutive laws can be conveniently applied according to the analysis considered in order to capture different phenomenological aspects. On one hand, it is possible to consider the blood flow as a Newtonian fluid for which we have the simplest model, usually used in good agreement with experimental data in major arteries. On the other hand, a non-constant value for the dynamic viscosity can also be used to model the blood behavior. An example of this kind of model is the Casson model. According to the case under study it may be more convenient to use a Newtonian or a Casson model. In this work we compare how flow pattern is affected into two different 3D models for the carotid bifurcation when changed the constitutive law of the blood. These models are embedded in a 1D model of the whole arterial tree. This embedding is performed through coupling conditions that makes both models well stated. Then, Newtonian and Casson models for the constitutive law of the blood are used to model the blood flow over a cardiac cycle. Flow patterns are compared for each case and some indicators are computed in order to have a better understanding on how these constitutive laws may lead to different results.

2 GOVERNING EQUATIONS

In this section the governing equations for each model, as well as boundary and coupling conditions used to close the system of equations are presented. A system of hyperbolic equations for the 1D model is provided. The corresponding system of equations for the 3D model is presented within the context of an ALE formulation due to the domain movement determined

by the wall movement. The latter is computed from a simple fluid-structure coupling scheme. Here, the blood's constitutive laws implemented are also presented, and some numerical aspects related to the Casson model are discussed.

2.1 1D model

The governing equations for the 1D model can be obtained by making appropriate assumptions over the momentum balance equations in their integral form. This system of equations govern the flow of an incompressible Newtonian fluid in compliant vessels. Considering the velocity profile as known, no flux across the wall, and assuming a cylindrical geometry for the vessel we obtain the following set of non-linear equations [17]

$$\frac{\partial A}{\partial t} + \frac{\partial Q}{\partial x} = 0, \tag{1}$$

$$\frac{\partial Q}{\partial t} + \frac{\partial}{\partial x}\left(\alpha \frac{Q^2}{A}\right) = -\frac{A}{\rho}\frac{\partial p}{\partial x} + f\frac{Q}{A}, \tag{2}$$

where A is the luminal area of the vessel, Q is the volume rate of blood, p is the blood pressure, ρ is the density of the fluid, x is an arbitrary point along the longitudinal axis, f is a coefficient that accounts for viscous terms and α is a correcting factor for the momentum due to the integration of the velocity profile over the area. For a fully developed parabolic profile we have $\alpha = \frac{4}{3}$ and $f = \frac{8\mu\pi}{\rho}$, with μ the dynamic viscosity of the fluid, although in this work $\alpha = 1$ was used. To close the system it is necessary to look for a $p - A$ relation that represents the wall behavior according to the blood pressure. In this regard, different models may be considered. The following viscoelastic model was used

$$p = p_0 + \frac{E\pi R_0 h_0}{A}\left(\sqrt{\frac{A}{A_0}} - 1\right) + \frac{k\pi R_0 h_0}{A}\frac{1}{2\sqrt{A_0 A}}\frac{dA}{dt}, \tag{3}$$

where index 0 refers to reference values, E is the effective Young modulus, k is the parietal viscosity and R and h are the wall radius and wall thickness respectively.

Note here that, although we compare different constitutive laws, for the 1D model we will always assume a Newtonian fluid, since our interest is just focused on how tridimensional flow patterns respond to changes in the constitutive law.

2.2 3D model

For the multidimensional domain we consider the variational formulation written in ALE form that reads as follows [11]: *find* $(\mathbf{u}, p) \in Kin_u \times Kin_p$ *such that*

$$\int_\Omega \rho \frac{\partial \mathbf{u}}{\partial t}\cdot \mathbf{v}\, d\Omega + \int_\Omega \rho\left((\mathbf{u}-\mathbf{w})\cdot\nabla\right)\mathbf{u}\cdot\mathbf{v}\, d\Omega - \int_\Omega p\ \mathrm{div}\,\mathbf{v}\, d\Omega + \int_\Omega \mu\nabla\mathbf{u}\cdot\nabla\mathbf{v}\, d\Omega = \int_{\Gamma_N}\mathbf{t}\cdot\mathbf{v}\, d\Gamma_N \qquad \forall \mathbf{v}\in Var_u, \tag{4}$$

$$\int_\Omega \mathrm{div}\,\mathbf{u}\ q\, d\Gamma = 0 \qquad \forall q \in Var_p, \tag{5}$$

where $\mathbf{u}$ is the fluid velocity, $\mathbf{w}$ is the domain velocity consistent with the ALE frame of reference, p is the blood pressure and ρ and μ the density and dynamic viscosity of the fluid. In this work volume force terms were disregarded and traction terms $\mathbf{t}$ over the Neumann boundary were added. Neumann boundary comprises just the coupling faces with the unidimensional model since essential conditions are taken for the vessel wall.

To solve the problem, a model for the wall must be furnished. This model provides essential boundary conditions over the velocity field $\mathbf{u}$. A simple model of independent rings was used for this purpose [15], and therefore the following set of equations have to be solved at each point of the boundary Γ_D (corresponding to the wall)

$$\begin{aligned} p &= p_0 + \frac{ER}{R_0^2}\gamma + \frac{kR}{R_0^2}\frac{d\gamma}{dt}, \\ \delta\mathbf{x} &= \gamma\mathbf{n}, \\ \mathbf{u} &= \frac{d\mathbf{x}}{dt}, \end{aligned} \tag{6}$$

where R is the radius at point $\mathbf{x}$, E and k as mentioned before, γ is the wall displacement and $\mathbf{n}$ is the outward normal vector.

Finally, a conduction problem for each degree of freedom corresponding to the domain displacements was implemented in order to propagate the wall displacements into the interior of the 3D domain.

2.3 Coupling conditions

To close the system of equations, some coupling conditions must be imposed in order to have both 1D and 3D models well posed. From the point of view of Euler equations we enforce mass continuity and normal stresses continuity. Thus, for the variational formulation (4)-(5) we have at each coupling interface Γ_i, $i = 1, \ldots, N_{cf}$ (N_{cf} the number of coupling faces) the following

$$Q_i + \int_{\Gamma_i} \mathbf{u}\cdot\mathbf{n}\, d\Gamma_i = 0, \tag{7}$$

$$\int_{\Gamma_N} \mathbf{t}\cdot\mathbf{v}\, d\Gamma_N = \sum_{i=1}^{N_{cf}} \int_{\Gamma_i} \mathbf{t}\cdot\mathbf{v}\, d\Gamma_i = \sum_{i=1}^{N_{cf}} \int_{\Gamma_i} p_i\mathbf{n}\cdot\mathbf{v}\, d\Gamma_i \qquad \forall \mathbf{v} \in Var_u, \tag{8}$$

where Q_i and p_i are mean quantities related to the unidimensional model (1)-(3) at the point corresponding to coupling boundary face Γ_i, whose outward normal is $\mathbf{n}$. See [4] for more details regarding coupling between models of different dimensionality.

2.4 Constitutive laws

Two constitutive laws are used with the purpose of quantifying the sensitivity of hemodynamic factors and flow patterns. The relation between stresses and strain rates is through the dynamic viscosity μ. For the Newtonian case this coefficient is constant, and hence a constant relation is obtained

$$\text{Newtonian constitutive law} \quad \rightarrow \quad \mu = \mu_o. \tag{9}$$

A more complex model may be regarded by means of the following expression

$$\text{Casson constitutive law} \quad \rightarrow \quad \mu(\hat{d}) = \left(\sqrt{\mu_o} + \sqrt{\frac{\tau_o}{2\hat{d}}}\right)^2, \tag{10}$$

where $\hat{d} = \sqrt{\frac{1}{2}\mathbf{d_u} : \mathbf{d_u}}$ is one of the invariants of the $\mathbf{d_u}$ tensor, that is the symmetric component of the velocity gradient. In model the constitutive (10), μ_o is the asymptotic value for the dynamic viscosity when $\hat{d} \rightarrow \infty$, while τ_o is the limit for $\hat{d} \rightarrow 0$. This model, known as

Casson model, carries out variations of the viscosity taking into consideration variations of the symmetric part of the gradient velocity tensor. Therefore, it must be expected some notorious variations in the velocity field when the strain rates tend to be negligible, since the viscosity for such situations grows considerably performing a rigid movement in the limit when no strain rate is present.

Notice that in the limit when $\hat{d} \to 0$ the model should be capable of modelling rigid movements. To handle numerically this drawback it is necessary to make some assumptions. In the present study, a regularization of the Casson model was performed by setting a high value for the viscosity when $\hat{d}$ reaches values below than a certain parameter. This limit parameter was progressively diminished in order to test the sensibility of the solution. The closer to zero the parameter is, the closer the regularized model is from the original model. These tests were carried out for the standard geometry and the regularization parameters found were used for the real geometry.

3 MODELS

In this section both models are presented, referencing the numerical techniques which were used for each case. For arterial tree model several aspects are discussed such as the imposition of boundary conditions. For the detailed multidimensional model of the carotid bifurcation a standard geometry and a real geometry are shown.

3.1 The Arterial tree

An approximation of the whole arterial system was obtained by considering a 128 segments[1] tree that represent the major arteries as shown in Figure 1(a). Geometrical and physiological parameters were taken from those proposed by Avolio [7]. For characterizing the parietal viscosity it is customary to define the viscoelastic angle as $\phi = \arctan\left(\frac{\omega k}{E}\right)$, where ω is related to the cardiac beat period T, $\omega = \frac{2\pi}{T}$. By setting the angle ϕ, the value for k can be computed for each segment according to the elastic parameter E. In this study we consider $\phi = 5^{\text{o}}$.

An inflow boundary condition for the flow ejected by the left ventricle of the aortic root was considered. In Figure 1(b) this boundary condition is displayed [18] through a cardiac cycle $T = 0.8\,sec.$ In order to take into account the interaction of the major vessels with the peripheral beds, lumped Windkessel models were implemented [8, 9, 10]. These models comprise three parameters, two resistances R_1 and R_2 and a capacitor C. The governing equation of this kind of model is given by the following expression

$$\frac{dQ}{dt} = \frac{1}{R_1 R_2 C}\left[R_1 C \frac{dp}{dt} + p - (R_1 + R_2)Q\right], \tag{11}$$

where, for a given pressure curve, this model returns the flow curve through that terminal. Here, values for R_1 and R_2 are set in order to have a correct blood flow distribution towards the different parts of the body (see for instance [1]), while values for C, that is, for the total peripheral compliance were determined according to criteria given in [9]. Finally, continuity on pressure and mass is held at bifurcations [8].

This model was discretized using 1212 nodes and 1326 linear elements. Equations (1)-(3) are discretized by means of the finite element method, using a Galerking Least-Squares technique over the characteristic lines corresponding to the normal equations associated with the resulting hyperbolic system when $k = 0$. Also, a θ-implicit scheme is considered. Such scheme is

[1] Each one representing an artery.

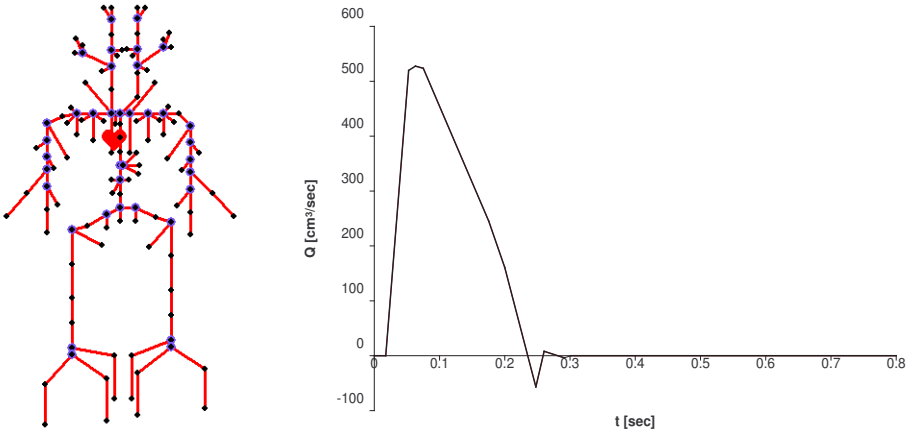

(a) 1D Tree topology. (b) Heart outflow curve.

Figure 1: One dimensional model.

operated with a stabilization parameter corresponding to the optimal value given for the SUPG method [2] and with θ close to $\frac{1}{2}$.

3.2 3D geometries

A natural approach for obtaining an approximate solution for this problem is the finite element method. Given a 3D domain, it is meshed with linear tetrahedral elements, and a P1b-P1 formulation is employed in order to circumvent spurious modes in the pressure field [3]. An arbitrary Lagrangian-Eulerian (ALE) formulation was implemented as mentioned before, and a SUPG method is used to avoid oscillatory solutions due to high convective terms. Here a θ-implicit method is considered due to the discretization of time derivatives through finite differences.

The coupled 3D-1D problem can be solved through a fully coupled algorithm computing both uni and multidimensional problems at the same time and solving quantities at coupling faces as a part of the system of equations. This approach has a high computational cost since the system requires a more efficient preconditioning process. Although this way is always preferred, sometimes highly coupled linear systems of equations appear as a result of refined multidimensional meshes. To avoid this kind of problem a decoupled algorithm may be more appropriated. This situation implies to solve alternatively the 3D model and the 1D model transferring information through coupling faces as boundary conditions. Nevertheless, sometimes it is crucial to set some sub-relaxation parameter between the iterations. In this work the last approach was taken. Thus, the solution of the problem is split into three sub-steps: in the first one, the bubble degrees of freedom are eliminated by direct substitution and the 3D problem (equations (4)-(6)) is solved using the pressure values obtained in 1D model in the previous time step as Neumann boundary conditions, and the domain displacements are then updated from the displacements of the nodes over the surface (see equation 6) by solving a Laplace problem for each nodal coordinate. In the second sub-step, the solution for the 1D model is computed with the flow rate values obtained from the multidimensional model in the first sub-step (equations (1)-(3)). Finally, in the third step, we solve the bubble degrees of freedom to be used in the following time step.

In next subsections the standard geometry (artificially generated from measures acquired in the literature) will be referred to as SG, while the real geometry (obtained from real patient

data) will be referred to as RG.

3.2.1 Standard geometry

The standard model for the carotid bifurcation was taken from [5, 6] and was scaled to be consistent with the diameter of the common carotid given by the unidimensional model. The geometry is depicted in table 1 and in Figure 2(a). The resulting finite element mesh has 57009 nodes and 323711 elements and is also presented in Figure 2(a).

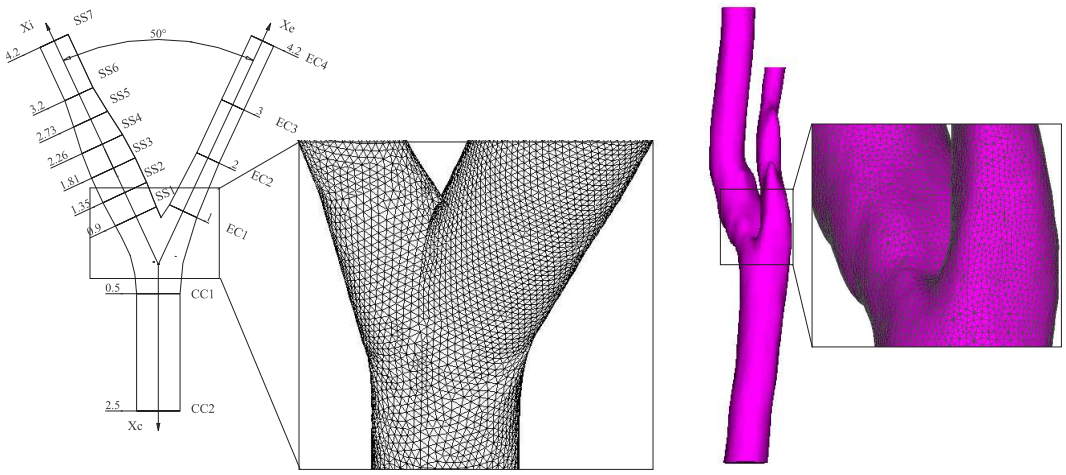

(a) Standard carotid geometry (SG) and mesh for the SG.

(b) Real carotid geometry (RG) and mesh for the RG.

Figure 2: Different geometries used.

Section	**SS1**	**SS2**	**SS3**	**SS4**	**SS5**	**SS6**	**SS7**
Diameter[cm]	0.77182	0.8214	0.8214	0.76368	0.6364	0.5254	0.5254
Section	**CC1**	**CC2**	**EC1**	**EC2**	**EC3**	**EC4**	
Diameter[cm]	0.74	0.74	0.51356	0.42032	0.42032	0.42032	

Table 1: Dimensions corresponding to standard geometry.

3.2.2 Real geometry

The real carotid geometry was acquired from a MRA. The input image was segmented using a novel segmentation method based on the Configurational Derivative [20]. From this segmentation, by means of Marching Cubes algorithm, the 3D mesh of the carotid artery internal wall was reconstructed. This initial mesh was post-processed to obtain the final surface mesh. From this triangular surface a tetrahedral mesh was constructed using a frontal method. The resulting finite element mesh has 94732 nodes and 638128 elements, and is presented in Figure 2(b).

4 RESULTS

For both models, computations were performed using a time step of $\Delta t = 1.25E-03\,sec$, and thus the cardiac cycle was divided into 640 steps. In the next subsections, results showing

differences between the Newtonian and the Casson model are presented. For each model, the oscillatory shear index (OSI) and the wall shear stress (WSS) are computed. The OSI measures the oscillation of shear stresses at the arterial wall and is computed from the following equation

$$OSI = \frac{1}{2}\left[1 - \frac{\left|\int_0^T \tau_w \, dt\right|}{\int_0^T |\tau_w| \, dt}\right], \tag{12}$$

where T is the cardiac period and τ_w is the stress at the artery wall. The WSS measures the mean shear stresses at the artery wall, and is obtained from the following equation

$$WSS = \frac{1}{T}\int_0^T |\tau_w| \, dt. \tag{13}$$

These indicators are important since they are believed to give idea of locations that tend to develop atheroma plaque deposition, and therefore stenosis growth [14, 15, 16].

It is worth mentioning that since the computation with the Casson model was not longer than the corresponding to the Newtonian model, employing the former could be considered more adequate.

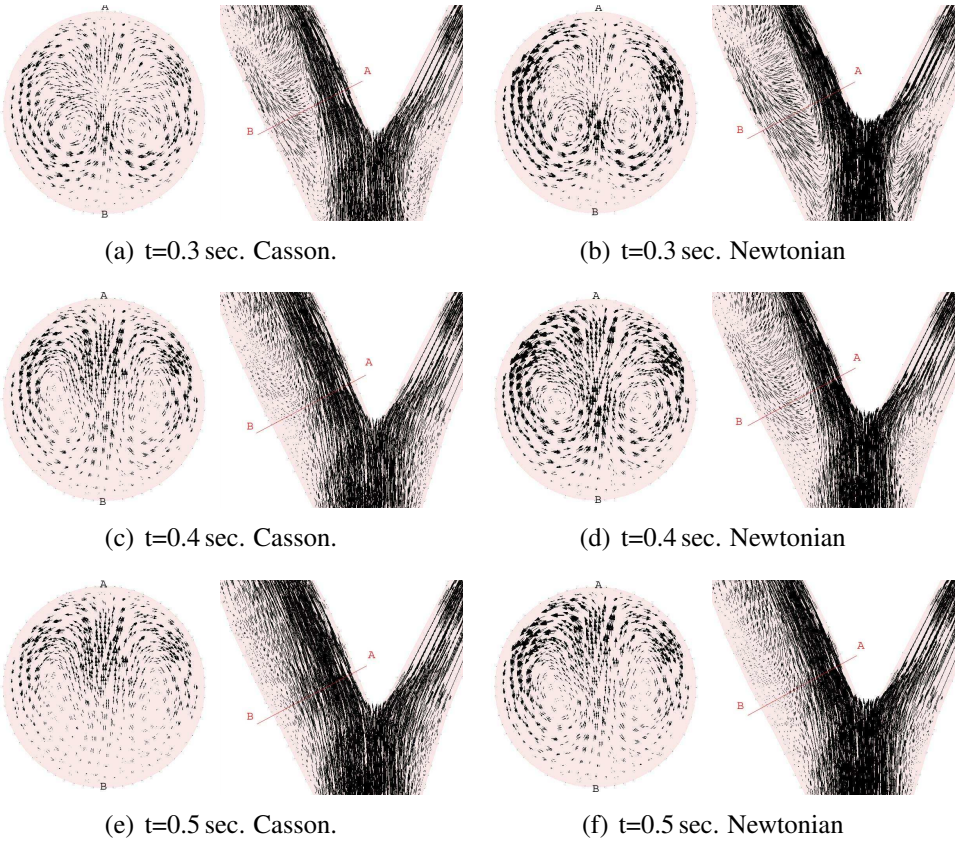

(a) t=0.3 sec. Casson. (b) t=0.3 sec. Newtonian

(c) t=0.4 sec. Casson. (d) t=0.4 sec. Newtonian

(e) t=0.5 sec. Casson. (f) t=0.5 sec. Newtonian

Figure 3: Transversal and longitudinal flow patterns for the SG.

4.1 Standard geometry

Figure 3 shows tangent velocity vectors at transversal section SS2 (see figure 2(a)) and the tangent velocity vectors at a longitudinal section as well. Vectors have been rescaled for each

time, but the scaling factor used is the same for both models. Point A indicates the inner wall side while point B is the corresponding outer wall side. In transversal sections it is possible to see that the vortex dynamics when considered Casson model is different from the Newtonian model. In the Casson model it seems to come out a more open secondary flow region in a radial direction of the inner wall side at $t = 0.3\,sec$ (see figure 3(a)). This is not observed in the Newtonian model where this flow region is more closed (see figure 3(b)). Likewise, it is appreciated that vortexes are more stretched for the Casson case, while for the Newtonian case they tend to remain circular. Regarding the longitudinal sections, after systolic phase it is observed that the effective area in the carotid sinus is bigger in the Casson model, or equivalently, the recirculating flow region is bigger for the Newtonian model. This can be also checked by results at $t = 0.4\,sec$ (figures 3(c) and 3(d)) and $t = 0.5\,sec$ (figures 3(e) and 3(f)). Also, it can be appreciated that the transversal flow is more accentuated in the Newtonian case. It stars with a high tangent velocity region over the laterals close to point A (see figure 3(b)) and continues to growth through all the inner side. In the Casson case the transversal flow is more regular at the beginning of the diastolic period (see figure 3(a)), while the growth of the tangent velocity field is not as stressed as in the Newtonian model.

Figure 4 displays the distribution of the OSI and the WSS index at the carotid sinus. For the Newtonian model it is observed a ring pattern of the OSI distribution, as a result of a higher recirculating flow region. Correspondingly, for the Casson model such a ring pattern does not appear, giving a more concentrated distribution for the OSI. Regarding the WSS index, for the Newtonian model there exist higher stresses that have a tendency to remain placed on the inner wall of the carotid bifurcation. This is direct consequence of a smaller effective area which the fluid flows through in the Newtonian case when compared with the Casson case.

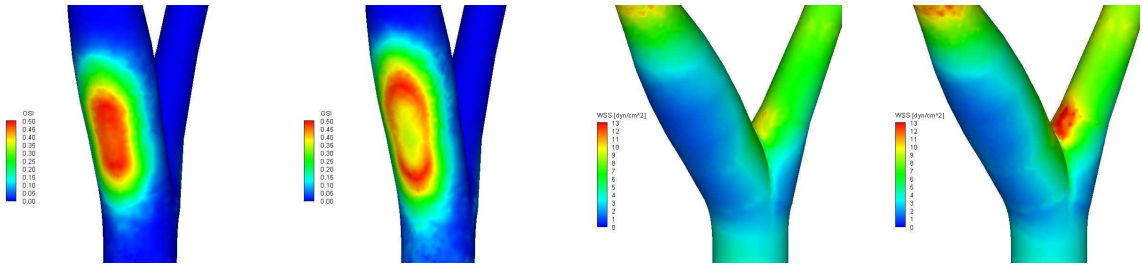

(a) OSI Casson. (b) OSI Newtonian. (c) WSS Casson. (d) WSS Newtonian.

Figure 4: OSI and WSS distributions for the SG.

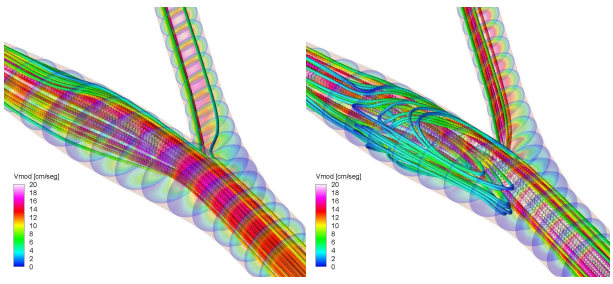

(a) Casson model. (b) Newtonian model.

Figure 5: Streamlines for the SG at $t = 0.3\,sec$.

To complement the presentation, in figure 5 the same streamlines at $t = 0.3\,sec$ were obtained for both models. It emphasizes differences between models, and stands out the higher recirculating flow region in the Newtonian case that generates the ring pattern for the OSI distribution seen in figure 4(b).

4.2 Real geometry

As flow patterns are closely affected by the geometry, in this case it is more difficult to establish a quantitative comparison such as the one carried out with the standard geometry. Nevertheless, it is possible to observe some characteristics corresponding to each model. The OSI and WSS distributions were computed, and are shown in figure 6. With regards to vortex dynamics, figure 7 presents the velocity field over transversal sections. Hence, it is more noticeable the dissimilarity between the Casson and the Newtonian models. In fact, flow pattern appears to be rather complex in the Newtonian case. Thus, results concerning OSI and WSS (see figure 6) are straightforward justified. The OSI parameter seems to reach very low values in the Casson case due to the well-behaved structure of the flow. The WSS distribution remains similar, in spite of the differences in maximum values. Here, the maximum value for the mean shear stress is in both cases located over the inner wall of the bifurcation, right at the front part of the geometry (the front part is the one shown in figures 6(c) and 6(d)).

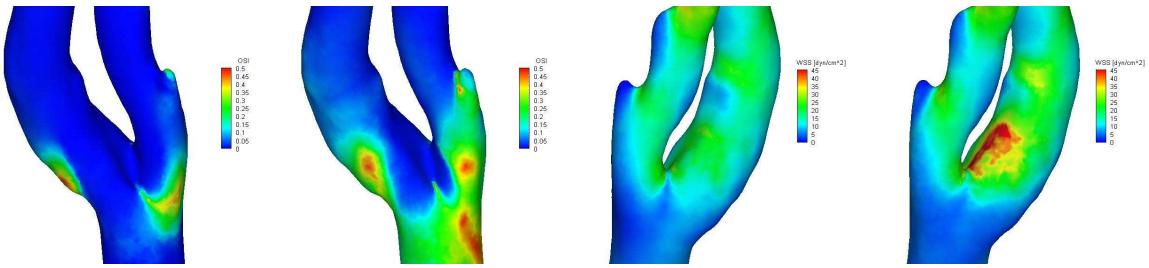

(a) OSI Casson. (b) OSI Newtonian. (c) WSS Casson. (d) WSS Newtonian.

Figure 6: OSI and WSS distributions for the RG.

A last word on these results. It was not disregarded that smaller regularization parameters were needed in order not to rigidify the solution. As mentioned, some tests were performed on the standard geometry to determine a correct regularization parameter for the Casson model, and the parameter chosen was used for computing in the real geometry. Nonetheless, as real geometry involves by far more complex flow patterns, it is possible to have reached the limit of the regularized Casson model in several parts of the domain, and therefore a more rigid solution was computed. Concerning this, some additional tests, in which we diminish even more the regularization parameter, are being carried out for the real geometry in this direction.

5 CONCLUSIONS

In this work, a comparison between two constitutive laws for modelling the blood behavior was presented by means of coupled 3D-1D models. Computations were performed on a standard and a real geometry. To quantify the sensitivity of the flow patterns to the constitutive law the OSI and the WSS indicators were used and some considerations over flow patterns were also given. A higher recirculating flow region was observed for the Newtonian model. A direct consequence of this is the alteration of the OSI indicator. Although the OSI indicator does

(a) Transversal velocity field for the Casson model.

(b) Transversal velocity field for the Newtonian model.

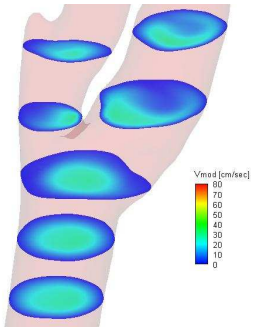

(c) Contours for the Casson model.

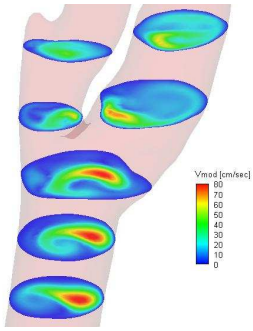

(d) Contours for the Newtonian model.

Figure 7: Transversal flow patterns for the RG at $t = 0.3\,sec.$

not present remarkable qualitative changes, the localization of maximum values for the Casson model is modified.

On the other hand, when considering real geometries using the Casson model appears to be the correct choice. Furthermore, these results show that, although an analysis in standard geometries may lead to important conclusions about the dynamics in a general situation. The development of a patient-specific modelling is justified when tempting to understand the dynamics that lag behind each particular case.

Concerning computation it is worthwhile to mention that computing with the Casson model does not take more time than the corresponding to the Newtonian model. Therefore, employing the former could be considered more adequate. In spite of this, some warnings must be given when regularizing the Casson model, since high values for the regularization parameter may lead to wrong solutions.

6 ACKNOWLEDGEMENTS

This research was partly supported by FINEP / CNPq - PRONEX Project under Contract 664007/1997-0, by MCT/PCI-LNCC Project. Pablo Javier Blanco (140686/2005-3) and Ignacio Larrabide (141336/2003-0) were partly supported by the Brazilian agency CNPq. The support of these agencies is greatly appreciated.

REFERENCES

[1] W.W. Nichols, M.F. ORourke, *McDonalds Blood Flow in Arteries: Theoretical, Experimental and Clinical Principles*. Fourth Edition, Arnold and Oxford Univ. Press, 1998.

[2] T.J.R. Hughes, A. Brooks, A theoretical framework for Petrov-Galerkin methods with discontinuos functions: Application to the stream-upwind procedure, *Finite Element in Fluids IV*, Wiley, London, 1982.

[3] O. Pironneau, *Finite-element methods for fluids*, Wiley, New York, 1989.

[4] S.A. Urquiza, P.J. Blanco, M.J. Vénere and R.A. Feijóo, Multidimensional modelling for the carotid artery blood flow, to be published in the *Comput. Meth. Appl. Mech. Engrg.*

[5] B.K. Bharadvaj, R.F. Mabon, D.P. Giddens, Steady flow in a model of the human carotid bifurcation, I. Flow visualisation, *J. Biomech.*, **15**, 349–362, 1982.

[6] B.K. Bharadvaj, R.F. Mabon, D.P. Giddens, Steady flow in a model of the human carotid bifurcation, II. Laser Doppler anemometer measurements, *J. Biomech.*, **15**, 363–378, 1982.

[7] A.P. Avolio, Multi-branched model of the human arterial system *Med. Biol. Engn. Comp.*, **18**, 709–718, 1980.

[8] M.S. Olufsen, Structured tree outflow condition for blood flow in large systemic arteries, *Am. J. Physiol.*, **276**, 257–268, 1999.

[9] N. Stergiopulos, D.F. Young, T.R. Rogge, Computer simulation of arterial flow whit applications to arterial and aortic stenoses, *J. Biomech.*, **25**, 1477–1488, 1992.

[10] F. Otto, Die Grundform des arteriellen pulses, *Zeitschrift für Biologie*, **37**, 483–529, 1899.

[11] T.J.R. Hughes, W.K. Liu, Zimmermann, Lagrangian-Eulerian finite element formulation for incompressible viscous flows, *Comput. Meth. Appl. Mech. Engrg.*, **29**, 329–349, 1981.

[12] L. Formaggia, F. Nobile, A. Quarteroni and A. Veneziani, Multiscale modelling of the circulatory system: a preliminary analysis, *Comput. Visual Sci.*, **2**, 75–83, 1999.

[13] L. Formaggia, J.F. Gerbeau, F. Nobile and A. Quarteroni, Numerical treatment of defective boundary conditions for the Navier-Stokes equations, *SIAM J. Numer. Anal.*, **40**(1), 376-401, 2002.

[14] D.P. Giddens, C.K. Zarins and S. Glagov, The role of fluid mechanics in the localization and detection of atherosclerosis, *J. Biomech. Engn.*, **115**, 588–594, 1993.

[15] A.S. Anayiotos, S.A. Jones, D.P. Giddens, S. Glagov and C.K. Zarins, Shear stress at a compliant model of the human carotid bifurcation, *J. Biomech. Engn.*, **117**, 98–106, 1994.

[16] D.N. Ku, D.P. Giddens, C.K. Zarins and S. Glagov, Pulsatile flow and atherosclerosis in the human carotid bifurcation. Positive correlation between plaque location and low oscillating shear stress, *Aterioscleroses*, **5**, 293–302, 1985.

[17] B.W. Schaaf, P.H. Abbrecht, Digital computer simulation of human systemic arterial pulse wave transmission: a nonlinear model, *J. Biomech. Engn.*, **5**, 345–364, 1972.

[18] J.C. Stettler, P. Niederer, M. Anliker, Theoretical analysis of arterial hemodynamics including the influence of bifurcations, *Annals of Biomedical Engineering*, 1980.

[19] S.A. Urquiza, P.J. Blanco, M.J. Vénere and R.A. Feijóo, Modelos multidimensionales de la bifurcación carotídia con diversos grados de estenosis. G. Buscaglia, E. Dari and O. Zamonsky eds. *ENIEF2004 - XIV Congress on Numerical Methods and their Applications*, Bariloche, Argentina, November 2004.

[20] I. Larrabide, R.A. Feijóo, E. Taroco, A.A. Novotny, Configurational Derivative as a Tool for Image Segmentation. C.A. Mota Soares et al. eds. *ECCM2006 - III European Congress on Computational Mechanics*, Lisbon, Portugal, June 2006.

[21] I. Larrabide, P.J. Blanco, S.A. Urquiza and R.A. Feijóo, Sensitivity of blood flow in stenosed carotid bifurcation. H. Rodrigues et al. eds. *ICCB2005 - II International Conference on Computational Bioengineering*, Lisbon, Portugal, September 2005.